Estudios Geológicos
julio-diciembre 2014, 70(2), e017
ISSN-L: 0367-0449
doi: http://dx.doi.org/10.3989/egeol.41730.323

LP-HT anatectic processes and lithological heterogeneity in the Mindelo Migmatite Complex (NW Portugal)

Procesos anatécticos (LP-HT) y heterogeneidad litológica en el Complejo Migmatítico de Mindelo (NW Portugal)

M. Areias[1], M.A. Ribeiro[1], J.F. Santos[2], A. Dória[1]

[1] Centro Geologia da Universidade do Porto. Email: mariaareias@fc.up.pt.com
[2] Geobiotec, Dep. Geociências. Universidade de Aveiro

ABSTRACT

The Mindelo Migmatitic Complex crops out in the coastal zone north of Porto (Portugal) and consists of a set of migmatitic and granitic lithologies. Field relationships, petrography, geochemistry and isotopic signature of the various lithologies allow inferring the sequence of anatectic processes that resulted in their characteristic lithological heterogeneity. The metasedimentary sequences (Schist-Greywacke Complex) show chemical composition and isotopic signature identical to the metatexites. So is suggested to be the protolith of Mindelo Migmatite Complex lithologies. The melting has occurred in several structural levels and thus at different pressure and temperature conditions, resulting in rocks with specific characteristics. In shallow levels (<3.5 kbar) metatexites are formed essentially by fluid-present partial melting followed by fluid-absent incongruent biotite melting producing peritectic cordierite, quartz, plagioclase and minor amounts of K-feldspar. The melt segregation led to its crystallization in dilatant sites forming masses and veins of leucogranite. In slightly deeper levels the melting rate is higher which leads to the formation of diatexites and two mica granites that intruded metatexites. This material rises in the crust and incorporates abundant xenoliths forming a very heterogeneous granitic body.

Tourmalinization of granitoids, migmatite and metasediments occurred at subsolidus conditions associated with aplite-pegmatites that cut all the other lithologies. A last aqueous fluid influx led to muscovitization of metatexites, granitoids and metasediments.

The migmatization started after the first ductile deformation phase of Variscan Orogeny (D_1) and was continuously active during the following stage of deformation and shear (D_3). The several pulses of different fluids that affected the Mindelo Migmatitic Complex probably are related to the emplacement of the syn and late- D_3 variscan granites.

The Mindelo Migmatite Complex represents an example of migmatites formed in low pressure conditions and illustrates some of the reactions involving melting in high grade pelitic rocks and subsequent mineral alterations due to infiltration of late different fluids.

Keywords: LP-HT migmatites; leucosomes; melt segregation

RESUMEN

El Complejo Migmatítico de Mindelo aflora en la zona costera de Portugal al norte de Oporto y se compone de un conjunto de litologías migmatíticas y graníticas. Las relaciones de campo, petrografía, geoquímica y las

Recibido el 1 de abril de 2014 / Aceptado el 11 de noviembre de 2014 / Publicado online el 09 de diciembre de 2014

Citation / Cómo citar este artículo: M. Areias et al. (2014). LP-HT anatectic processes and lithological heterogeneity in Mindelo Migmatite Complex (NW Portugal). Estudios Geológicos 70(2): e017. http://dx.doi.org/10.3989/egeol.41730.323.

características isotópicas de las diferentes litologías permiten inferir la secuencia de procesos anatécticos que dio lugar a su típica heterogeneidad litológica. La composición química e isotópica de la secuencia metasedimentaria del Complejo Esquisto-Grauváquico es idéntica a la de las metatexitas, lo que sugiere que sea el protolito de las litologías del Complejo de Mindelo.

La fusión se ha producido en varios niveles estructurales y por lo tanto en diferentes condiciones de presión y temperatura, dando lugar a rocas con características específicas: i) en niveles relativamente superficiales (<3,5 kbar), las metatexitas se forman principalmente por fusión parcial húmeda seguida de fusión incongruente de biotita produciendo cordierita peritéctica, cuarzo, plagioclasa y cantidades menores de feldespato potásico. Los leucogranitos y venas de leucogranito son consecuencia de la migración de leucosomas. En niveles ligeramente más profundas la tasa de fusión es superior, lo que conduce a la formación de diatexitas y de granitos de dos micas que intruyen a las metatexitas. Este material se eleva en la corteza e incorpora abundantes xenolitas formando un cuerpo granítico muy heterogéneo.

La turmalinización de leucogranitos, granitos de dos micas, migmatitas y metasedimentos tuvo lugar en condiciones subsolidus, asociada a aplitas/pegmatitas que cortan al resto de litologías. Una última entrada de fluidos acuosos condujo a la moscovitización de metatexitas, granitoides y metasedimentos.

La migmatización comenzó después de la fase de engrosamiento cortical de la Orogenia Varisca y estuvo activa durante la siguiente etapa de deformación y cizalla. Los pulsos de diferentes fluidos que afectaron el Complejo Migmatítico de Mindelo probablemente están relacionados con el emplazamiento de los cuerpos graníticos sin y tardi -D_3.

El Complejo Migmatítico de Mindelo representa un ejemplo de migmatitas formadas en condiciones de baja presión e ilustra algunas de las reacciones que implican la fusión de rocas pelíticas en alto grado y sus alteraciones minerales posteriores debido a la infiltración de diferentes tipos de fluidos.

Palabras clave: LP-HT Migmatitas; leucosomas; segregación de fundido

Introduction

The Mindelo Migmatite Complex (MMC) is a migmatite massif associated with a syn-orogenic granite in the western border of the Central Iberian Zone (CIZ), the axial zone of the Iberian Variscan Orogen (Fig.1A). In the Variscan Belt the metamorphism occurred mostly under low pressure and high temperature (Martínez *et al*., 2001; Valle Aguado *et al*., 2005; Ribeiro *et al*., 2008; Catalán *et al*., 2014). In CIZ the high-grade rocks, belonging mainly to the Schist-Greywacke Complex (SGC), are associated with peraluminous granitic plutons and anatectic complexes, materializing thermal domes developed in a late stage of the Variscan Orogeny (Escuder Viruete *et al*., 1994; Martínez *et al*., 2001; Bea *et al*., 2003; Valle Aguado *et al*., 2005; Ribeiro *et al*., 2008; Catalán *et al*., 2014). The association of amphibolite facies metamorphic rocks with migmatites grading into granitic rocks has been described in different sectors of the Iberian Variscan Belt (Pereira & Bea, 1994; Barbero & Villaseca, 1995; Valle Aguado *et al*., 2010). The MMC is one of these migmatite complexes.

This paper aims to infer the protolith and sequence of anatexis processes that gave rise to the migmatization and production of various granitic rocks that crop out in Mindelo Migmatitic Complex based on field relationships, petrography, geochemistry and isotopic signature.

Geological setting

The Central Iberian Zone (CIZ), the axial zone of the Iberian Variscan Orogen represents a piece of the external margin of northern Gondwana, involved in the Paleozoic collision with Laurentia after the closure of the Rheic Ocean (Ribeiro *et al*., 2007 and references therein). In the Iberian Variscan Belt the main deformation phase (D_1) affected all the pre-Carboniferous sedimentary sequences and produced NW–SE sub-vertical folds with an axial planar slaty cleavage or schistosity. This is the main foliation observed in the field. Continuous to D_1 a second deformation phase (D_2) manifests mainly through movements along the base of sub-horizontal major thrusts (Noronha *et al*., 1979; Noronha *et al*., 2000). These events were followed by a predominantly extensional phase, named D_2 by some authors (Valle Aguado *et al*., 2005) that allowed anatexis in the middle crust and segregation of magmas. These anatectic magmas rise at the beginning of D_3 leading to the emplacement of large volumes of peraluminous granites (Noronha *et al*., 1979; Casquet *et al*., 1988; Escuder Viruete, *et al*., 1994; Díez Balda *et al*., 1995; Ábalos *et al*., 2002; Azevedo & Valle Aguado, 2013). D_3 produced asymmetric, kilometric-scale sub-vertical folds with NW–SE to NNW– SSE axial planes. These folds commonly show a poorly developed axial

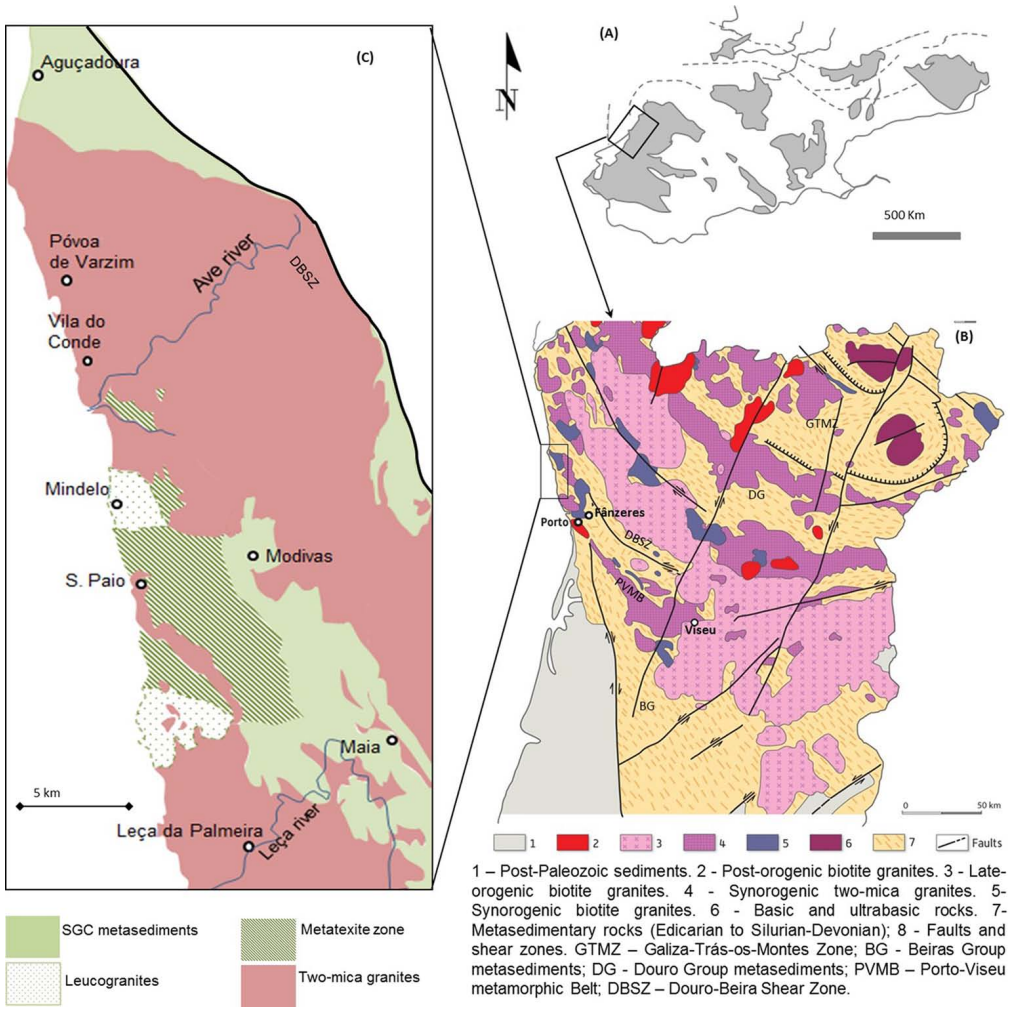

Fig. 1.—Geological sketch and location of the study area. A) European Variscan massif; B) Simplified geological map of northern Portugal with the representation of the main granite types and metasedimentary rocks; C) Geolgical sketch of the Mindelo Migmatite Complex.

planar crenulation cleavage and vertical or steeply plunging axes (Noronha *et al*., 1979; Ribeiro *et al*., 2008; Romão *et al*., 2013). A complex D_3 strike-slip shear zone network was active and reactivated for a long time, during and after the variscan collision. These shear zones controlled the fluid-flow that had an important role in metamorphic, metasomatic and metallogenetic processes (Noronha *et al*., 2000, 2013).

The MMC is situated on the northeast part of Porto-Viseu metamorphic belt (Azevedo & Valle Aguado, 2013). This NW-SE antiformal megastructure has a core composed by syntectonic anatectic granites intimately associated with HT-LP migmatites: MMC in the area under study and Mundão Anatectic Complex near Viseu (Valle Aguado *et al*., 2010) (Fig. 1). Towards the flanks the metamorphic grade decreases rapidly.

The magmatic activity that prevailed during the variscan orogenic cycle developed along different deformational stages. Thus, the magmatic rocks mainly represent orogenic granitoids, which are defined according to different age groups. In recent years both geochronological and structural data point to the definition of several intrusion times for iberian granitic rocks, which can be divided in three major groups: pre-orogenic granites, orogenic granites and post-orogenic granites (Ferreira *et al*., 1987; Díez Balda *et al*., 1995; Valle Aguado *et al*., 2005; Martins *et al*., 2011; Azevedo & Valle Aguado, 2013)

(Fig. 1B). According to their chemical and mineralogical composition, the variscan granitoids can be grouped into two families: peraluminous, two-mica granites and leucogranites and biotite (±Crd±Hnb) granodiorites. The widespread occurrence of Crd-bearing granites has led some petrologists to suggest an intermediate series or family of "granites of mixed features" (Capdevila *et al*., 1973; García-Moreno *et al*., 2007). Most of leucogranites are related to the principal metamorphic episodes and their emplacement is associated with the last deformation phase (D_3) and the development of ductile extensional shear zones (Ferreira *et al*., 1987; Escuder Viruete *et al*., 1994; Díez Balda *et al*., 1995; Valle Aguado *et al*., 2005; Azevedo & Valle Aguado, 2013). They are spatially related to low-pressure, high-temperature anatectic domains. Bt-rich granodiorites are mainly late with respect to the main deformation phases and are associated with strike slip faults and crustal-scale shear zones (Casquet *et al*., 1988; Martins *et al*., 2011).

Several authors and the published geological maps (Teixeira & Medeiros, 1965; Pereira *et al*., 1992) ascribe the MMC metasedimentary rocks to the Schist Greywacke Complex (SGC). The Schist-Greywacke Complex is a thick turbidite sequence aged Ediacaran to Cambrian that occupies the major part of the Central Iberian Zone. Two main units have been recognized: a lower unit aged Ediacaran and an upper unit aged Early Cambrian (Valladares *et al*., 2000; Ugidos *et al*, 2010; Pereira *et al*., 2012). In Portugal these two units were nominated Beiras Group (BG) and Douro Group (DG) respectively (Sousa, 1984) (Fig. 1).

Very low to low-grade metamorphism prevails in wide areas of the Schist-Greywacke Complex, except in the vicinity of the syntectonic anatectic granites, where the field gradient is marked by condensed isograds. These isograds are parallel to the granite bodies, ranging in a short distance from chlorite to sillimanite zone (Ribeiro *et al*., 2008) prevailing moderate to low-P metamorphic conditions.

Rock types and field relationships in the Mindelo Migmatite Complex

In the Mindelo Migmatite Complex appear distinct lithologies, both of sedimentary and magmatic origin, namely: patch metatexites, banded metatexite, diatexites, metagreywacke and calc-silicate resisters, leucogranites, two-mica granites and aplite-pegmatites. The unmigmatized rocks from the Schist Greywacke Complex surrounding MMC were also studied in order to understand their relationship with the migmatites.

Schist-greywacke Complex Metasediments

The Schist-Greywacke Complex in the vicinity of the MMC is composed essentially by alternating metapelites and metagreywackes (some of them with calc-silicate nodules), varying in thicknesses from centimetric to metric (with metapelite in higher proportion) (Areias *et al*., 2012). The main cleavage observed in the field is related to the D_1 deformation phase. From east to west the metamorphic grade increases from chlorite to biotite, staurolite and sillimanite zones passing gradually to migmatites (Fig. 1C). In this paper we have studied the staurolite-schists in the vicinity of MMC (Aguçadoura, Fig. 1C) and the staurolite-schists from Fânzeres, some kilometres to the southeast (Fig. 1B).

These rocks show biotite-rich bands and quartz-plagioclase-rich bands. Large poikilitic staurolite crystals include euhedral garnet, ilmenite and round quartz. Late andalusite and cordierite develops in the biotite-rich bands. A retrograde paragenesis is marked by chlorite replacing garnet and muscovite/sericite replacing plagioclase, biotite, andalusite, staurolite and cordierite. There are abundant late tourmaline and apatite.

The Aguçadoura staurolite-schists are closer to the granites and their paragenesis is richer in late andalusite and cordierite than that of staurolite-schists from Fânzeres. The adjacent granites have abundant xenoliths of schists.

Patch and banded metatexites

Patch migmatites and banded metatexites outcrop in the central part of the MMC, designated Metatexite Zone (Fig. 1C). Patch migmatites (PMM) dominated by paleosome, are characterized by the occurrence of small scattered patches of neosome resulting from discrete partial melting (Fig. 2A). Patch migmatites are rare and occur always associated with thick metagreywacke resisters layers that inhibit more widespread partial melting in these rocks.

Fig. 2.—Field pictures of the Mindelo Migmatite lithologies. A) Patch-migmatite; B) Banded metatexite and transverse leucogranite dike. These dikes are apparently discordant but they exhibit petrographic continuity (similar microstructure and mineralogy) with concordant leucosome; C) Diatexite with schlieren (indicated by white arrows); D) Leucogranite with K-feldspar in miarolitic cavities; E) Two-mica granite; F) Metatexite xenolith within two-mica granite.

Banded migmatites (BMM) where the neosome portion increases show a roughly dark and light layered structure generally concordant with the main regional cleavage (S_1). Most of them consist of discrete discontinuous centimetric-thick layers of medium grained leucosomes alternating with millimetric to centimetric thick biotite and sillimanite-rich melanosomes (Fig. 2B).

Leucosomes are coarse grained, white-pink coloured and can be classified using a two-fold division based on relationships with surrounding banded metatexites – they are either concordant or discordant to local foliation. Concordant leucosomes are in petrographic continuity with discordant leucosomes (with similar microstructure and mineralogy) (Fig. 2B). Leucosome filled shear zones and leucosomes parallel to axial surfaces of D_3 folds are common.

The migmatite leucosomes materialize folds correlated to the D_3 dextral transcurrent shear zones, but these leucosomes do not show solid-state deformation.

The melanosomes show anastomosed foliation marked by aligned biotite and sillimanite. They contain biotite + sillimanite + garnet + quartz + oligoclase + cordierite + secondary muscovite. Zircon, monazite, apatite and ilmenite are widespread accessory minerals. Garnet is fully or partially replaced by cordierite + quartz + sillimanite and is restricted to melanosomes. Biotite shows symplectitic textures, anhedral shape and is replaced by cordierite, K-feldspar or quartz. Most of the cordierite is located in the boundary between melanosome and leucosome.

Leucosomes show large quartz + plagioclase ± K-feldspar crystals. These large crystals include small grains of anhedral or rounded quartz, plagioclase, biotite and accessory minerals. Fragments of melanosome are entrained in the leucosome. There are melanocratic selvedges with biotite + cordierite + sillimanite ± garnet surrounding the patch leucosomes (Fig.2A).

The K-feldspar is very rare in patch migmatites and in some banded migmatites (in some of them was detected only in backscattered images) and is always replacing plagioclase. It is possible to find metatexites without any K-feldspar crystal close to K-feldspar bearing metatexites less than 3 m away from each other. It is noteworthy that the calc-silicate resisters in metatexites without K-feldspar show no replacement textures or mineralogy; however, those inserted in K-feldspar bearing migmatites show obvious signs of local retrograde replacement (Areias *et al*., 2012).

Both, leucosomes and melanosomes show several textures typical of partial melting, namely magmatic microstructures in leucosomes (Fig. 3), quartz or K-feldspar films surrounding the biotite grains (Figs. 3A and 3B), magmatic rims on subsolidus cores of grains (*e.g*. magmatic rims of plagioclase$_2$ and K-feldspar enclosing anhedral remnant plagioclase$_1$) (Fig. 3C), presence of peritectic cordierite (Fig. 3B) and plagioclase, quartz and K-feldspar cuspate grains (Fig. 3D).

Diatexites

Diatexites (DTX) show a magmatic texture and pre-partial-melting structures are generally absent. They are mesocratic although with colour variations. Several biotite schlieren stand out as dark alignment within the rock (Fig. 2C). Diatexites crop out within the metatexite both as bodies with few tens of square meters and as metric thick veins cutting metatexites. In both cases the contact between diatexites and metatexites is abrupt.

Diatexite matrix consists of medium grained quartz + plagioclase + K-feldspar + biotite. The schlieren that are the melt-depleted remains of pelitic layers are composed of aligned biotite + sillimanite + cordierite ± garnet. The amount of accessory minerals such as monazite, zircon and apatite is relatively high. The garnet is rare, anhedral and corroded and it is always associated with the schlieren. The diatexites show similar mineral composition and mineral relations to the banded metatexites, although they have much higher leucosome/melanosome ratio.

Leucogranite

The leucogranites (L.Gnt) crop out immediately north and south of migmatites where appear as bodies with several tens of square meters, but they also occur as veins cutting the metasedimentary sequence (SGC) in the vicinity of the migmatite complex. They are characterized by its whitest colour and scarcity of biotite or other dark minerals. The rare biotite and sillimanite usually are clustered in spots. The field appearance is very similar to most of the leucosomes although peritectic cordierite, abundant in the *in situ* leucosomes and diatexites is absent in leucogranite. The transition of metatexites to leucogranites is gradual: the proportion of melanosome gradually decreases from metatexites with melanosome dominant to leucogranites with abundant restites and leucogranites with few clusters of biotite and sillimanite. Unlike the diatexites and two-mica granites have sharp contact with the metatexites.

Leucogranite are composed of quartz + plagioclase + biotite ± K-feldspar ± garnet ± muscovite (sec.) ± chlorite (sec.). Garnet is very sporadic, corroded and fine grained and its composition is quite similar to the composition of garnet in schists and melanosomes. These features suggest a restitic character of the garnet crystals and the same is pointed for biotite and sillimanite in clusters. Biotite and garnet are replaced by chlorite and muscovite. Locally the biotite clusters disappear and instead there are tourmaline + K-feldspar + quartz symplectitic clusters with the same texture and structure as the biotite clusters, forming tourmaline bearing leucogranites (TL.Gnt).

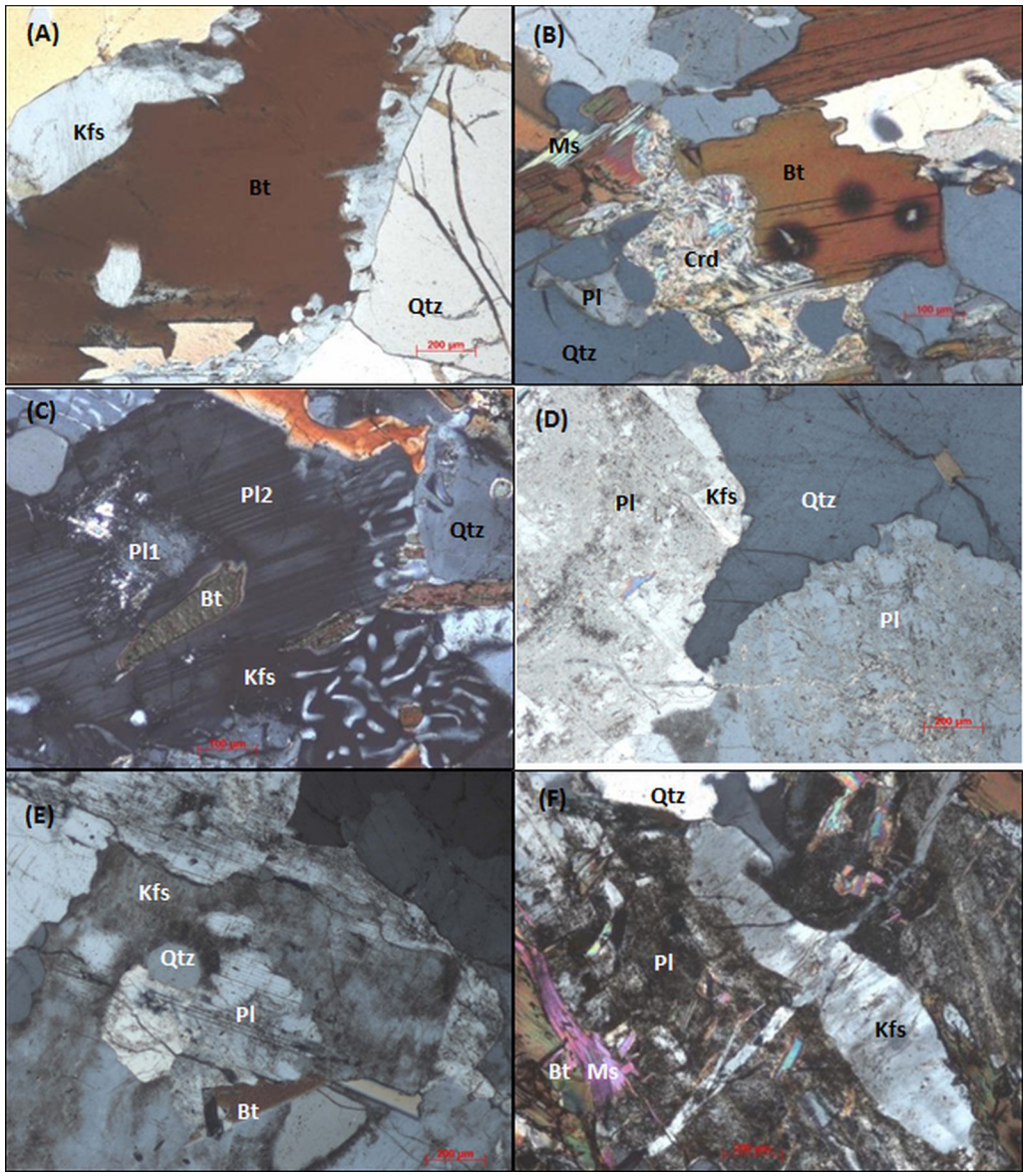

Fig. 3.—Photomicrographs of MMC lithologies showing partial melting textures (A to D) and metasomatic textures (E and F). A) K-feldspar concentrated in films surrounding the biotite grains and euhedral quartz (banded metatexite); B) Cordierite replacing biotite and anhedral plagioclase inside quartz crystal (patch metatexite); C) Residual biotite and plagioclase (Pl_1) inside neo-formed plagioclase (Pl_2) and symplectitic intergrowths of quartz and feldspar nucleating on euhedral crystals of plagioclase; D) Grains of plagioclase separated by elongate and cuspate grains of quartz and feldspar; E) K-feldspar replacing plagioclase; F) K-feldspar veins cutting plagioclase crystal.

Like leucosomes, there are leucogranites with abundant K-feldspar and leucogranites with rare K-feldspar. In fact, all the leucosome and leucogranite samples with K-feldspar show textural evidence of plagioclase replacement by K-feldspar, namely K-feldspar with plagioclase cores (Fig. 3E), plagioclase inclusions in K-feldspar which are in parallel optical continuity with a plagioclase crystal outside the K-feldspar, microfractures filled with K-feldspar (Fig. 3F) and development of large crystals of K-feldspar in miarolitic cavities (Fig. 2D).

Two-mica granites

Two-mica granites (2m.Gnt) crop out north, south and east of leucogranites and migmatites and also as smaller bodies (hundred square meters) within migmatites (Fig. 2E). There are several granitic dikes

and veins, generally fine-grained or porphyritic that cut the migmatites and even the metasedimentary sequence in the vicinity of migmatites. The two-mica granite bodies include fragments (xenoliths) of metagreywacke and calc-silicate resisters as well as metatexites (Fig. 2F).

They are composed of quartz + plagioclase + K-feldspar + biotite + muscovite + apatite + zircon + monazite ± andalusite ± tourmaline. Some of them still have rare aligned schlieren with biotite + sillimanite ± garnet. Tourmaline only occurs locally and most of muscovite, although abundant, is secondary.

Geochemistry

Whole-rock major and trace element analyses were carried out by ICP and ICP-MS (inductive coupled plasma / mass spectrometry) at "Activation Laboratories" (Ancaster, Ontario) (Table 1).

Migmatites

One of the most striking features in metatexites is the variation in Ca, Sr, Mn and Na content. Ca ranges from 0.35 to 1.89 (wt.%) and Na from 0.79 to 3.22 (wt.%). The content of Ca is directly correlated with Na and Sr contents ($r^2=0.88$ and $r^2=0.86$ respectively). The greater amount of Ca and Na are in those metatexites in the vicinity of greywacke resisters and could result from partial melting of external portions of the greywacke layers. The pelite rocks from the SGC show the same variation on those elements (Ca, Na, Sr and Mn). Fig. 4A shows a multivariate diagram for average composition of pelitic rocks of the SGC (n=4) and of metatexites (n=4). Values are normalized to NIBAS (Ugidos, *et al*., 2010) and show that both metatexites and SGC samples have major and minor elements similar to the NIBAS standard (exception for slight variations in Mn, Ca, Na, Sr).

Diatexites show depletion in Fe, Mg, Mn (V, Co) and all the HSFE relatively to SGC and metatexites (Fig. 4B).

Leucosome shows the same variation relatively to the metatexites but even with higher depletion in ferromagnesian and "HFS" elements (Fig. 4C).

High variability in K_2O content is observed in metatexites (2.4 to 6.1 wt.%), which is reflected by the abundance of K-feldspar in the respective leucosomes. Also the K content is higher in calc-silicate resisters located in the vicinity of K-feldspar bearing migmatites.

The occurrence of both melt-rich and melt-depleted metatexites is reflected in their chemical composition; the last show lower SiO_2, Na_2O and CaO and higher Fe_2O_3t + MgO, Ba and Rb contents relatively to the protolith. The segregation and migration of melt at some points and accumulation in others was probably promoted by differential deformation in the metatexites. Metatexites in the vicinity of the leucogranite bodies show darker colour and high melanosome/leucosome ratio. These features are consistent with residual composition and substantial leucosome extraction and consequent enrichment in biotite, sillimanite, garnet and cordierite.

Metatexite REE pattern (chondrite normalized; Boynton, 1984) is similar to SGC samples and NIBAS (Fig. 5). It is characterized by high total REE content, negative Eu anomaly and moderately REE fractionation, presenting a typical shale REE pattern. The diatexite REE pattern has a peculiar shape: the REE content is lower than metatexite, there is no Eu anomaly and the HREE fractionation is higher. The leucosome pattern shows the lower REE total content, positive Eu anomaly and moderate HREE fractionation (Fig.5).

Leucogranite and leucogranite veins

Leucogranite composition is quite similar to the concordant leucosome, although with some variability (Fig. 4C). Like leucosome they are depleted in Fe, Mg, Mn, HFSE, Co and V relatively to the other lithologies and NIBAS. The leucocratic veins show even high depletion in these elements, especially those that intruded away from the metatexite zone (both in metasediments and in granites). They are characterized by low Fe_2O content (<2 wt.%), SiO_2 range from 71 to 78 wt.% and high variability in K_2O content ranging from 1.4 to 7.3 wt.%. The K_2O content is inversely correlated with $CaO + Na_2O$ content.

A notable feature is the remarkable enrichment in Rb, Nb and Ta and the depletion in Ba in the tourmaline bearing leucogranites relative to the others leucogranites (Fig. 4C).

The leucogranite REE pattern is similar to the concordant leucosome, showing low total REE content, positive Eu anomaly and low HREE fractionation

Table 1.—**Major (wt. %) and trace elements (ppm) compositions of MMC**

Type	SGC	PMM	BMM	BMM	BMM	BMM	BMM	BMM	BMM	BMM	BMM	BMM	BMM	DTX	LCS	L.Gnt	2m.Gnt
Sample	Av.	VC28	FM23	FM4	VC6	VC27	FM18	FP46	FP46	FM16	FP21	FM22	Av	Av.	Av.	Av.	Av.
	n=4												n=10	n=5	n=2	n=7	n=13
SiO_2	61.0	61.0	55.4	59.2	63.8	67.7	71.9	64.3	65.9	68.4	65.1	68.4	65.0	72.9	71.7	74.5	72.6
Al_2O_3	19.8	19.3	21.0	17.7	16.2	14.7	13.6	14.7	14.3	15.4	15.2	15.0	15.8	14.0	15.0	14.1	14.7
Fe_2O_3t	7.1	8.5	8.8	8.2	7.5	5.9	3.9	6.5	5.4	4.3	6.3	4.3	6.1	2.1	1.6	0.8	1.4
MnO	0.0	0.1	0.1	0.1	0.1	0.1	0.0	0.1	0.1	0.1	0.1	0.0	0.1	0.0	0.0	0.0	0.0
MgO	2.1	2.9	3.4	3.2	2.9	2.0	1.5	2.5	2.0	1.7	2.6	1.6	2.3	0.7	0.6	0.2	0.4
CaO	0.2	0.5	0.4	1.1	0.7	0.4	1.3	1.3	2.2	1.6	1.9	1.3	1.2	0.9	0.6	0.4	0.5
Na_2O	1.0	1.0	1.4	2.1	1.7	1.4	2.7	2.5	3.1	2.6	3.2	2.3	2.3	2.3	2.2	3.6	2.8
K_2O	3.3	3.7	6.1	3.4	3.6	3.5	2.5	2.8	2.1	3.1	2.7	4.0	3.4	4.5	6.7	4.2	5.2
TiO_2	0.8	1.1	1.1	1.0	0.9	0.8	0.6	0.9	0.9	0.5	0.8	0.6	0.8	0.3	0.2	0.1	0.2
P_2O_5	0.1	0.2	0.1	0.2	0.1	0.1	0.1	0.2	0.2	0.3	0.2	0.4	0.2	0.2	0.3	0.2	0.4
Sc	19.0	21.0	24.0	20.0	17.0	17.0	10.0	17.0	16.0	9.0	15.0	12.0	15.7	5.2	3.5	2.1	2.6
Be	3.0	2.0	2.0	2.0	3.0	1.0	2.0	3.0	3.0	8.0	3.0	2.0	2.9	3.6	3.5	7.9	5.1
V	162	156	150	167	131	112	55	127	106	66	112	72	110	33	15	9	14
Ba	690	794	1006	380	584	571	289	365	394	445	498	600	513	726	1086	407	284
Sr	59	119	90	144	126	93	180	143	165	190	243	201	158	182	221	139	63
Y	28	39	27	26	26	29	17	23	26	19	33	30	26	17	13	6	7
Zr	194	279	173	288	215	224	236	203	195	215	196	216	216	119	20	29	84
Rb	130	148	237	164	169	205	107	177	118	110	225	127	164	115	131	163	269
La	35.4	41.4	49.3	54.4	38.0	37.7	33.3	29.6	24.1	31.6	34.0	35.1	36.7	20.2	8.4	5.5	15.4
Ce	72.1	85.5	98.9	109.0	79.3	76.4	67.2	62.5	53.7	63.8	73.3	71.6	75.6	41.4	17.7	10.6	34.4
Pr	8.7	10.1	11.6	12.5	8.8	8.5	7.7	7.6	6.2	7.5	8.2	8.4	8.7	4.7	2.0	1.2	4.2
Nd	33.7	40.9	42.7	47.9	34.2	32.2	28.5	28.8	24.3	27.8	32.8	31.6	33.1	18.1	7.9	4.5	17.0
Sm	7.0	9.0	8.2	9.5	7.0	6.6	5.6	6.1	5.2	5.9	7.0	6.8	6.8	4.0	2.0	1.1	4.1
Eu	1.4	1.2	1.3	1.4	1.5	1.3	1.2	1.4	1.5	1.3	1.4	1.4	1.4	1.2	1.4	0.5	0.5
Gd	6.2	6.9	6.5	7.6	5.9	5.1	4.4	5.1	4.6	5.1	6.5	6.1	5.7	3.6	2.1	1.0	3.2
Tb	1.0	1.2	1.0	1.1	0.9	0.8	0.7	0.8	0.8	0.8	1.1	1.1	0.9	0.6	0.5	0.2	0.4
Dy	5.7	7.2	5.4	6.0	5.3	5.0	3.8	4.5	4.6	4.6	6.5	6.3	5.2	3.3	2.7	1.1	1.9
Ho	1.1	1.5	1.1	1.1	1.1	1.1	0.7	0.8	0.9	0.8	1.3	1.2	1.0	0.6	0.5	0.2	0.3
Er	3.3	4.4	3.1	3.2	3.1	3.3	1.9	2.4	2.7	2.0	3.7	3.0	2.8	1.7	1.4	0.6	0.6
Tm	0.5	0.7	0.5	0.5	0.5	0.6	0.3	0.4	0.4	0.3	0.5	0.5	0.4	0.2	0.2	0.1	0.1
Yb	3.3	4.4	3.0	3.2	3.0	3.7	1.7	2.7	3.1	1.5	3.5	2.6	2.8	1.5	1.3	0.6	0.5
Lu	0.5	0.7	0.5	0.5	0.5	0.6	0.3	0.5	0.5	0.2	0.6	0.4	0.4	0.2	0.2	0.1	0.1
Hf	5.2	7.1	5.0	7.5	5.6	5.3	6.4	5.1	4.4	6.2	5.2	5.9	5.7	3.1	0.6	1.0	2.4
Ta	0.9	0.9	2.3	1.2	0.9	1.0	0.8	1.0	0.8	0.8	1.0	1.1	1.1	0.5	0.4	1.1	1.0
Nb	11.8	14.0	29.0	16.0	13.0	11.0	12.0	12.0	10.0	11.0	13.0	14.0	14.1	5.2	3.5	3.4	6.7
Th	10.3	13.3	16.7	16.8	11.1	11.0	12.2	8.4	7.0	10.8	9.2	12.1	11.5	6.9	2.4	1.8	8.4
U	3.5	3.8	5.3	4.8	3.0	3.5	4.2	2.8	2.6	4.4	3.5	4.3	3.8	3.2	1.8	2.6	7.2

SGC: Schist-Greywacke Complex; PMM: Patch metatexites; BMM: Banded metatexites; DTX: Diatexites; LCS: Leucosomes; L.Gnt: Leucogranites; 2m.Gnt: Two-mica granites; Av: average; n: nº of samples.

(Fig. 5). Among leucosomes, those with the lowest ΣREE have marked positive Eu anomaly and a moderately fractionated REE pattern (La_N/Sm_N = 3.5–4.4), while those with the highest ΣREE show slight positive Eu anomaly and a slightly less fractionated REE pattern (La_N/Sm_N = 2.7–3.4). The leucogranite veins have the lowest REE content and the highest Eu anomaly.

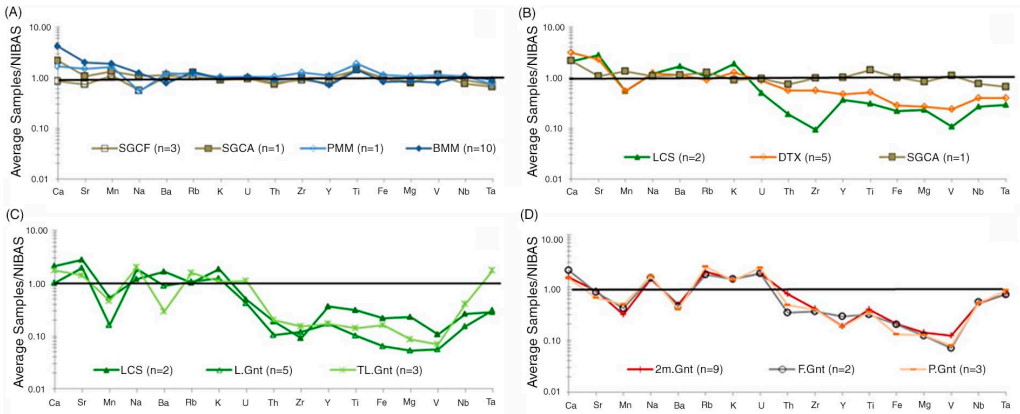

Fig. 4.—Multielement diagrams normalized to NIBAS (Ugidos, 2010) for the MMC lithologies. (A) SGCF: SGC pelites from Fânzeres; SGCA: SGC pelites from Aguçadoura; PMM: patch migmatites; BMM: banded metatexites. B) LCS: leucosomes; DTX: diatexites; SGCA: SGC pelites from Aguçadoura. C) LCS: leucosome; L.Gnt: leucogranites; TL.Gnt: tourmaline leucogranites. D) 2m.Gnt: two-mica granites; F.Gnt: fine-granites; P.Gnt: porphyry granites (data from Ferreira, 2011).

Two-mica granites

Two-mica granites, fine-grained granites and porphyritic granites show similar chemical composition (Fig. 4D). Relatively to diatexite they are slightly depleted in Fe, Mg, Mn, Ca, Sr, Ba, Y, V and Co and enriched in P, K, Rb, Ta, Nb, U and Th. The Fe_2O_{3t} content ranges from 1.33 to 1.99 wt.%, similar to that of leucogranites although slightly higher. SiO_2 rages from 70.4 to 74.4 wt.% and K_2O average is 5.2 wt.%. In this lithology the K_2O content is not correlated with $CaO+Na_2O$ content.

The REE pattern is typical of granites (Fig. 5), showing moderate REE content (lower than migmatites), marked Eu negative anomaly, moderate LREE fractionation and high HREE fractionation.

All the granitic lithologies (diatexites, leucogranites, two-mica granites, fine-grained granites and porphyritic granites) are highly peraluminous being the excess Al accommodated in phases like muscovite, andalusite, sillimanite or cordierite. The SiO_2 content is high (69–78 wt.%) what classifies the granitic rocks as granites. However, two-mica granites show moderate K_2O content and low variation (4.6–5.9 wt.%), diatexites show lower K_2O content (3.54–4.85 wt.%) and leucogranites show high K_2O variability (1.44–7.73 wt.%) (Table 1).

For granitic melts, Rb, Sr and Ba provide critical constraints on the conditions that prevailed during melting whereas REE are primarily controlled by accessory phase behaviour (Harris & Inger, 1992). The representation of the MMC granite rocks on the Ba-Rb-Sr ternary diagram (El Bouseily & El Sokkary, 1975, Fig. 6) does not reflect a clear differentiation trend. Diatexites, leucosome and leucogranites are mainly clustered in the anomalous-granite field. The pelitic metatexites plot in the same field. Two-mica granites plot in the field of normal granites and show a differentiated trend. Leucogranites with tourmaline plot in the field of highly differentiated rocks as well as aplite-pegmatite. This has not relation with K_2O content since there are differentiated leucogranites both with rare K-feldspar and with abundant K-feldspar. However there is correlation with the high abundance of tourmaline, muscovite and Ta + Nb content of these lithologies.

Sr and Nd isotopic signatures

Twenty-nine samples were selected for Rb-Sr and Sm-Nd isotope studies from the MMC and the SGC (Table 2). The analyses were performed in the laboratory of Isotope Geology, University of Aveiro. For initial ratio calculations a 325 Ma age is assumed since this is the age used by several authors considering the emplacement age of most syn-tectonic variscan granites (Beetsma, 1995; Teixeira, 2008, Teixeira *et al.*, 2012).

Sr-Nd isotopic signatures show a substantial crustal component for all the MMC lithologies, including granite, migmatites and metasedimentary rocks showing εSr_{325} values ranging from 114 to 262 and εNd_{325} values ranging from −9.3 to −2.1.

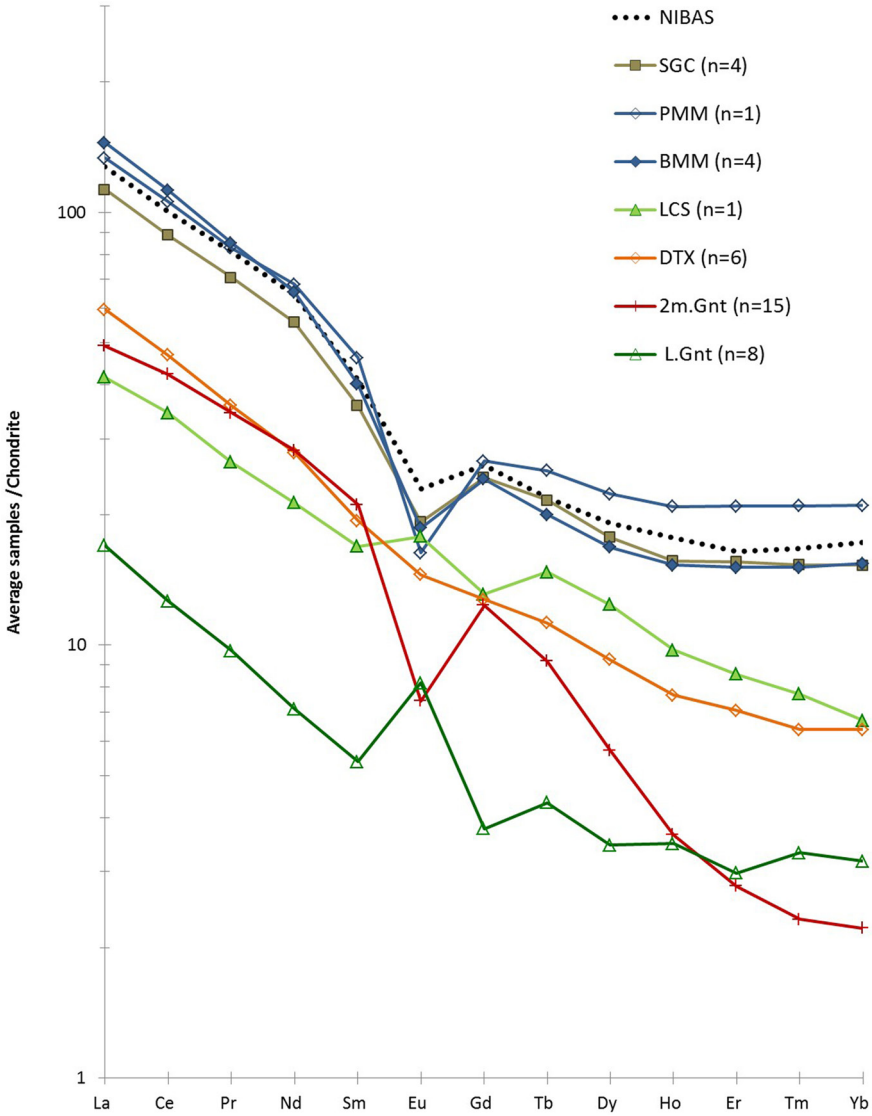

Fig. 5.—(A) Chondrite-normalized (Boynton, 1984) REE patterns of the MMC lithologies. NIBAS: Neoproterozoic Iberian Average Shale (Ugidos *et al.*, 2010); SGC: Schist-Greywacke Complex; PMM: patch migmatites; BMM: banded metatexite; LCS: leucosomes; DTX: diatexites; 2m.Gnt: two-mica granites, fine granites and porphyry granites; L.Gnt: leucogranites.

The SGC show relatively wide ranges of initial $^{87}Sr/^{86}Sr$ (0.71328–0.80369), as reported by other authors for these metasediments (Ugidos, *et al.*, 2003; Beetsma, 1995, Teixeira, 2008). These values clearly indicate disturbance of the Rb-Sr system. The Rb-Sr system may be perturbed by source-rock weathering, K metasomatism and Rb mobility during diagenesis. The MMC lithologies (migmatites and granites) show much shorter range of initial $^{87}Sr/^{86}Sr$. This suggests that the Rb-Sr recycling system was complete during the anatectic process.

The range of $^{147}Sm/^{144}Nd$ values for all the analysed samples are within the limits established by Zhao *et al.* (1992) for undisturbed clastic sediments (from 0.100 to 0.130). The samples can be divided into two groups: Group I comprise the SGC schists, the patch-metatexites and all the granitic rocks, showing εNd_{325} values between −2.1 and −5.4; Group II includes metagreywacke and calc-silicate resisters showing εNd_{325} values between −8.2 and −9.3. The banded migmatites have values ranging between these two groups. The aplite-pegmatite samples show values outside both groups with εSr_{325}~70 and εNd_{325}~−6.0 (Fig. 7A).

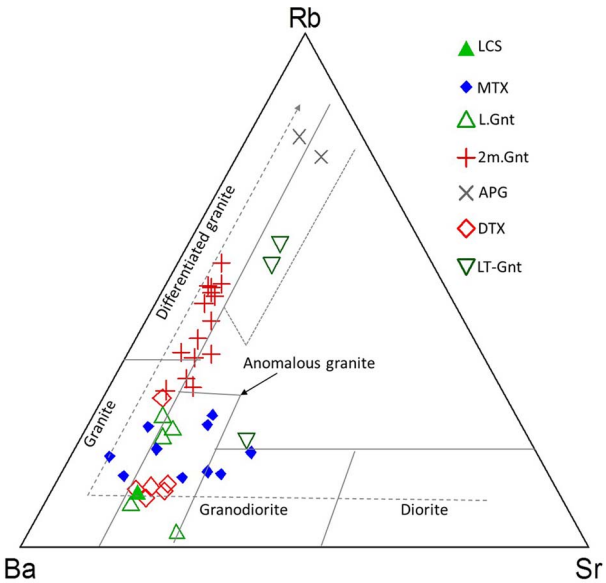

Fig. 6.—Ba-Rb-Sr ternary diagram (El Bouseily & El Sokkary, 1975) for the MMC lithologies. LCS: leucosome; MTX: patch and banded metatexites; L.Gnt: leucogranites; 2m.Gnt: two-mica granites; APG: aplite-pegmatites; DTX: diatexites; TL.Gnt: leucogranites with tourmaline.

Discussion

Nature of the migmatite sources

The field relationships, the identical chemical composition and the lithological similarities between the SGC and the metatexites, namely the occurrence of shales, greywackes and calc-silicate rocks, suggest a genetic relationship between the migmatites of the MMC and the SGC.

The isotopic composition of the MMC samples, compared with the values obtained by other authors for the granitic and metasedimentary rocks of the CIZ in the diagram εSr_{325} *versus* εNd_{325} (Fig. 7A), show that the SGC schists of the Group I (comprising the SGC schists, the patch-metatexites and all the granitic rocks of MMC) coincide with the values found by Beetsma (1995) for Beiras Group (SGC.bg). The metagreywacke (GWK) and the calc-silicate resisters (CSR), belonging to Group II with lower εNd_{325} values, are close to the compositional field defined by Teixeira (2008) for Douro Group (SGC. dg).

The Nd isotope composition of terrigenous sediments is controlled by two mains: (1) mixing of detrital components derived from ancient and juvenile source rocks in the provenance area; and (2) mechanical sorting and quartz dilution effects during erosion, transport and deposition resulting in unmixing of provenance components (McLennan, 1989). The bimodal Nd isotope variability between the two main groups is related with different type of terrigenous metasediments in these two groups – Group I comprise pelitic metasediments that resulted mainly from authigenic deposition of clays and group II comprise Ca metagreywackes composed mostly by allogenic material transported from elsewhere.

The dispersion of the Nd isotope composition in banded metatexites probably relates to the intrinsic characteristics of this type of lithology that comprises a restite portion (paleosome) and a newly formed fraction (neosome). More likely is that the restite portion maintains the isotopic signature while the newly formed portion will have an isotopic signature derivative from the phases involved in the melt formation (Barbero & Villaseca, 1995). Confirming this hypothesis is the fact that leucosomes, leucogranites and two-mica granites show similar εNd_{325} (Fig. 7A). Granitoids were subjected to high rate of melting and subsequent integration of all components. So even if derived from a heterogeneous isotopic source, will produce a relatively homogeneous isotopic signature. Patch metatexites have very low rate of melt production and no melt migration so will also have a homogeneous isotopic signature, which should be close to the protolith.

The relation $^{86}Sr/^{87}Sr$ versus 1/Sr is used to better understand the genetic relation between the MMC different lithologies. The schist from Aguçadoura, the migmatites (metatexites and diatexite), the leucogranites and the two-mica granites form a linear correlation ($r^2=0.93$) on the $^{86}Sr/^{87}Sr$ versus 1/Sr diagram (Fig. 7B). The SGC from Fânzeres and aplite-pegmatites plot outside the trend-line. Metagreywackes, although next the migmatites, show more spreading pattern. A deformed sample of two-mica granite shows high $^{87}Sr/^{86}Sr$ values (0.80369) (Fig. 7B).

The relative isotopic homogeneity among the MMC lithologies and the metasediments outcropping north of the MMC suggests a direct genetic relationship between two-mica granites, leucogranites, migmatites and the SGC that outcrop in the vicinity of the migmatite complex. The metasedimentary

Table 2.—**Rb-Sr and Sm-Nd data for MMC**

Lithology	Sample	Sr ppm	Rb ppm	$^{87}Rb/^{86}Sr$	2σ	$^{87}Sr/^{86}Sr$	2σ	Nd ppm	Sm ppm	$^{147}Sm/^{144}Nd$	2σ	$^{143}Nd/^{144}Nd$	2σ
SGC	**FM14**	70	105	4.351	0.123	0.734	2E-05	32.4	6.8	0.12695	4.E-03	0.51231	2.E-05
SGC	**FM15**	75	59	2.281	0.065	0.728	2E-05	15.6	3.3	0.12796	4.E-03	0.51229	2.E-05
SGC	**FM38a**	49	78	4.622	0.131	0.743	2E-05	33.8	6.9	0.12349	7.E-03	0.51224	2.E-05
SGC	**VC65**	84	161	5.567	0.157	0.748	2E-05	31.9	6.9	0.13084	7.E-03	0.51232	2.E-05
PMM	**VC37**	298	153	1.487	0.042	0.719	2E-05	34.6	7	0.12238	7.E-03	0.51237	2.E-05
PMM	**VC28**	119	148	3.606	0.102	0.729	2E-05	40.9	9	0.13100	7.E-03	0.51236	2.E-05
BMM	**FM4a**	144	164	3.302	0.093	0.730	1E-05	47.9	9.5	0.11997	3.E-03	0.51217	2.E-05
BMM	**VC 27b**	93	205	6.401	0.181	0.745	2E-05	32.2	6.6	0.12399	7.E-03	0.51224	2.E-05
BMM	**FM 16**	190	110	1.677	0.047	0.722	2E-05	27.8	5.9	0.12838	4.E-03	0.51208	1.E-05
BMM	**FM23**	90	237	7.651	0.216	0.751	2E-05	42.7	8.2	0.11616	3.E-03	0.51208	2.E-05
BMM	**FM 22**	201	127	1.831	0.052	0.724	2E-05	31.6	6.8	0.13017	4.E-03	0.51212	2.E-05
DTX	**VC 60**	215	134	1.806	0.051	0.721	2E-05	22.5	4.6	0.12367	7.E-03	0.51236	2.E-05
LCS	**VC8**	190	129	1.968	0.056	0.724	2E-05	12.8	3.3	0.15595	4.E-03	0.51233	1.E-05
L.Gnt	**FM19**	252	133	1.529	0.043	0.722	2E-05	3	0.7	0.14114	4.E-03	0.51224	2.E-05
L.Gnt	**VC2a**	94	139	4.293	0.121	0.742	2E-05	7	1.8	0.15555	8.E-03	0.51237	1.E-05
TL.Gnt	**VC 52**	58	215	10.784	0.305	0.764	2E-05	4.1	1.1	0.16229	1.E-02	0.51231	2.E-05
2m.Gnt	**FP21a**	67	254	11.032	0.312	0.767	3E-05	17.3	4.5	0.15734	4.E-03	0.51235	1.E-05
2m.Gnt	**FP21b**	90	191	6.160	0.174	0.741	2E-05	16.8	4.3	0.15483	4.E-03	0.51229	1.E-05
2m.Gnt	**VC22**	69	208	8.763	0.248	0.756	2E-05	30.3	6.3	0.12577	4.E-03	0.51228	2.E-05
2m.Gnt	**VC 39**	89	229	7.474	0.211	0.748	2E-05	18.8	4.8	0.15444	8.E-03	0.51232	1.E-05
2m.Gnt	**VC 45**	49	330	19.668	0.556	0.804	2E-05	27.4	6.1	0.13467	7.E-03	0.51230	1.E-05
CSR	**FM21a**	213	30	0.408	0.012	0.713	3E-05	34.7	7.4	0.12900	4.E-03	0.51207	1.E-05
CSR	**VC50a**	139	18	0.375	0.011	0.714	1E-05	34.3	6.8	0.11992	6.E-03	0.51203	2.E-05
CSR	**VC50b**	287	35	0.353	0.010	0.713	2E-05	27.3	5.5	0.12187	7.E-03	0.51200	1.E-05
GWK	**FM21b**	274	76	0.803	0.023	0.716	2E-05	26	5	0.11633	3.E-03	0.51205	2.E-05
GWK	**VC50c**	203	79	1.127	0.032	0.719	1E-05	26.3	5.2	0.11960	6.E-03	0.51200	2.E-05
GWK	**VC 47**	185	77	1.206	0.034	0.720	2E-05	27.2	5.2	0.11564	6.E-03	0.51201	2.E-05
APG	**VC58**	36	182	14.836	0.420	0.778	2E-05	2.1	0.6	0.17283	2.E-02	0.51226	2.E-05
APG	**VC64**	32	264	24.355	0.689	0.822	4E-05	1.4	0.5	0.21604	2.E-02	0.51238	2.E-05

SGC: Schist-Greywacke Complex (metapelites); PMM: Patch metatexites; BMM: Banded metatexites; DTX: Diatexites; LCS: Leucosomes; L.Gnt: Leucogranites; TL.Gnt: Tourmaline leucogranites; 2m.Gnt: Two-mica granites; CSR: Calc-silicate rocks; GWK: Metagreywackes (SGC); APG: Aplite-pegmatites.

rocks that outcrop further south, in the Fânzeres area, although they have the same source did not directly participate in the production of migmatites and granites of the MMC. The aplite-pegmatite samples seems to be related to the syn-tectonic (syn-D_3) granites since they plot outside the MMC groups within the field of syn-tectonic granites defined by Beetsma (1995).

REE patterns and accessory phase's entrainment

Many investigators have shown that a large part of the total budget of some trace elements, including REE, Y, Th, U, Hf and Zr is located in accessory minerals and the behaviour of these minerals during partial melting largely controls the way trace elements are distributed between the anatectic melt and the residuum

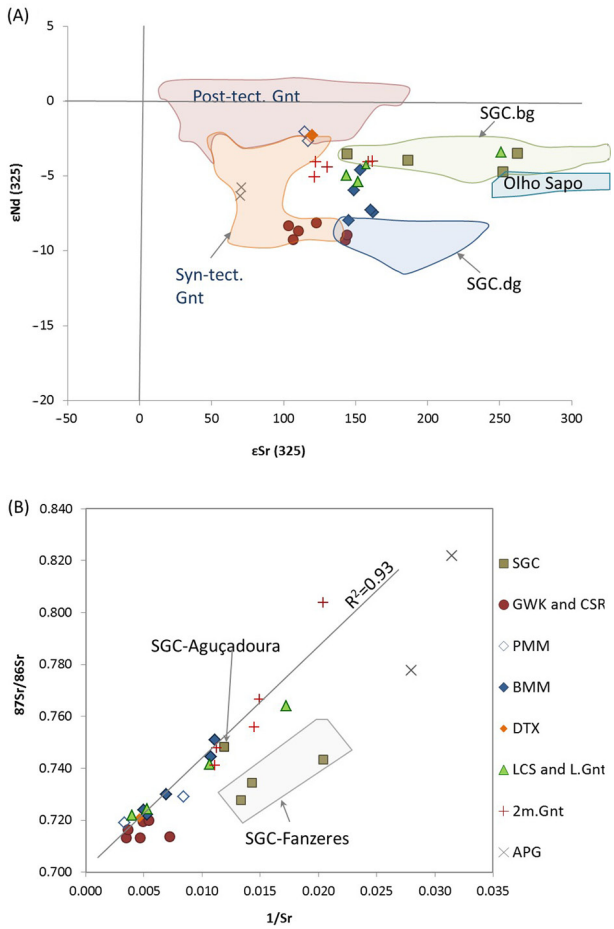

Fig. 7.—A) Plot of MMC rocks in the εSr_{325} *versus* εNd_{325} diagram. The shaded areas are the fields defined by Beetsma (1995) for the syn-tectonic granites (Syn-tect Gnt), post-tectonic granites (Post-tect. Gnt), Schist-Greywacke Complex – Beiras Group (SGC.bg) and for Schist-Greywacke Complex - Douro Group (SGC.dg), by Teixeira (2008). B) 1/Sr versus $^{87}Sr/^{86}Sr$ diagram for the MMC rocks. SGC: Schist Greywacke Complex; GWK: metagreywacke resisters; CSR: calc-silicate resisters; PMM: patch metatexites; BMM: banded metatexites; DTX: diatexites; LCS: leucosomes; L.Gnt: leucogranites; 2m.Gnt: two-mica granites; APG: aplite-pegmatites.

(Bea 1996; Watt *et al*., 1996; Bea & Monteiro, 1999). These processes are clearly observed in the MMC. In migmatites (including patch metatexite, banded metatexite and diatexite) the total REE content is positively correlated with Zr, Th and Y content (r^2=0.79, 0.90 and 0.78 respectively). Leucogranites also show positive correlation between Zr, Th and Y (r^2=0.95, 0.89 and 0.77 respectively). In two-mica granites the positive correlation is not so strong and is especially related to Th content (r^2=0.89) (Figs. 8A and B).

The Eu anomaly is linked to the preponderant role of accessory minerals with respect to plagioclase. The lower the Th and Zr content the less is the negative Eu anomaly in migmatites and two-mica granites. The leucogranites and leucosomes, with positive Eu anomaly, show the minor amount of these elements. The Na_2O/CaO ratio is inversely correlated with Eu positive anomaly.

In migmatites the Zr and Th contents are positively correlated with Fe_2O_3+MgO contents (r^2=0.63 and 0.69 respectively). Two-mica granites also show this positive correlation but it is notorious the abrupt enrichment in Th that does not follow the trend of other lithologies (Figs. 8C and D). However the LREE content of two mica granites and diatexites is similar (Fig. 5). In migmatites the LREE fractionation is directly correlated to Th content (r^2=0.6) and HREE fractionation is inversely correlated with the Y content (r2=0.7). However, in two-mica granites no correlation is observed. This suggests that Th in two-mica granites is not exclusively associated with monazite. This could be related to the fact that monazite and zircon commonly have different average grain size, and probably monazite was preferentially dissolved in granite since the differential flux of trace elements into the melt during dissolution of accessory phases is a function of dissolution rate and surface area, which are correlated to grain size and the degree of under-saturation of the melt with respect to the element(s) concerned (Watson, 1996).

It is clear that the relationship between the dissolution of accessory minerals in the melt influences the content and pattern of REE. Moreover, these minerals are closely related to the only ferromagnesian mineral present, i.e. biotite. However, in two-mica granites, higher dissolution of monazite liberated Th in the melt.

Melting processes

Field relationships, whole-rock chemistry and isotopic signature suggest that SGC was the protolith of the MMC lithologies. One of the most distinctive aspects of the MMC granitic rocks is their lithological, mineralogical and textural variation. The chemical and mineralogical dissimilarity between the MMC granitic rocks could result from their derivation from different crustal levels, different fusion

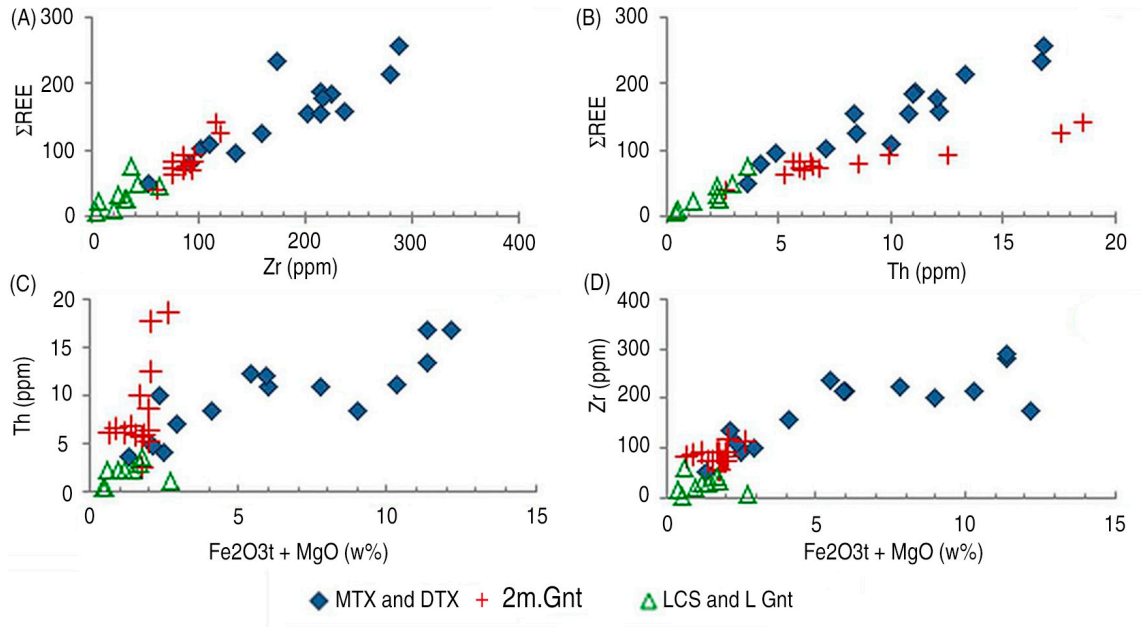

Fig. 8.—A and B - Bivariate diagrams Zr and Th *versus* ∑REE for MMC lithologies. C and D – Bivariate diagrams Zr and Th *versus* Fe_2O3_t + MgO. MTX: metatexites; DTX: diatexites; 2m.Gnt: two-mica granites; LCS: leucosome; L.Gnt: leucogranites.

rates and/or different melt segregation process rather than of a marked difference in the source lithologies involved.

The leucogranite and leucogranite veins composition, namely the high HSFE depletion relatively to metatexites and the distinct REE patterns can be produced by removal of leucosome before complete equilibration due to the inhibited dissolution of accessory phases, during an early stage of segregation and extraction (Barbero & Villaseca, 1995; Watt *et al*., 1996; Zeng *et al*., 2005a and 2005b; Brown, 2008, 2013). Evidence for channelized flow and deformation-enhanced melt segregation on an outcrop scale is present all over the MMC where melt migration occurs over several distances.

It is likely that a first fluid-present melting pulse takes place in the MMC and produced most of the leucosomes, leucogranites and leucogranite veins. As referred before, leucosomes and leucogranites show high variability in the K_2O content and consequent heterogeneity in K-feldspar abundance. The K content is inversely correlated with $Na_2O + CaO$ content what is reflected by the replacement of plagioclase by K-feldspar in these lithologies. The K-poor leucosomes and leucogranites are a possible outcome of the SGC metasediments H_2O-melting, in an earliest stage, at relatively low T, during prograde conditions, as postulated by several authors (Conrad *et al*., 1988; Patiño Douce & Harris, 1998; García-Casco *et al*., 2001, Jung, 2005; Zeng *et al*., 2005b). Fluid-present melting, which mainly consumes plagioclase and minor amounts of mica, will produce strong Sr enrichment and marked Rb and Ba depletion (Harris & Inger, 1992). MMC leucogranites are characterized by low Rb/Sr values, much lower than the two-mica granite values (average Rb/Sr = 1.07 and 4.44 respectively) and higher Ba/Sr values (average Ba/Sr = 0.38 to leucogranites and 0.22 to two-mica granites). The positive Eu anomaly observed in most leucosomes and leucogranites also argues in favour of prevailing fluid-present, inasmuch as fluid-absent melting is known to yield negative Eu anomalies (Harris & Inger, 1992). It is also significant that the leucosomes and leucogranites are cordierite-free, as opposed to what occurs in diatexites. The first result from fluid-present melting and the second are the product of fluid-absent hydrate-breakdown melting that carry anhydrous (peritectic) minerals, such as cordierite or garnet or pyroxene (Milord *et al*., 2001; Brown, 2013).

The availability of water for melting reactions decreases since water is rapidly dissolved into the

melt. Thus, and in agreement with the observed textures, the migmatization continues by fluid-absent biotite breakdown reactions (Brown, 2008; White, 2008):

$$Bt + Pl_1 + Sil + Qtz = Crd + Pl_2\ (\pm Kfs) + Melt \quad (1)$$

$$Bt + Sil + Qtz = Crd + Kfs + Melt \quad (2)$$

Reaction (1) and (2) take place in relatively shallow crustal levels. The peritectic cordierite and the absence of peritectic garnet or ortopyroxene (either in metapelites or in metagreywackes) indicate that melt occurred at P<4 kbar and T<760 °C (assuming that chemical equilibrium is attained; White, 2008).

The diatexites show mineralogical and chemical composition coherent with *in situ* partial melting containing all the same mineral phases as the banded migmatites but the leucosome/melanosome ratio is much higher with consequent relatively low ferromagnesian elements and HSFE content. They show the sequential evolution from low melt fraction metatexites to high melt fraction diatexites. The absence of resisters within diatexites and its higher Ca content is an outcome of calc-silicate greywackes incorporation in their composition, which gives it a calc-alkaline character. This suggests that the melting temperature was probably slightly higher for diatexites than metatexites and consequently the melting rate. The abrupt contacts between diatexites and metatexites suggest that the diatexites intruded metatexites and have been formed at deeper levels. However the P-T conditions and melting reactions of diatexites and migmatites formation were not much different since the mineralogy is identical.

In the MMC several factors must be taken into account with regard to the relationship between granites and migmatites: (1) two-mica granites have a truly intrusive character; there are sills, dikes and other bodies that cut the migmatite rocks and incorporate migmatite xenoliths; (2) its wall rocks (metasediments and metatexite) are mostly poor in potassium and usually their only potassium-rich mineral is biotite; therefore, the huge amounts of potassium-rich granite cannot result exclusively from segregation *in situ;* (3) the mineralogical and chemical composition of two-mica granites is different from that of migmatites and leucogranites. The former have andalusite which is absent in migmatites and have more K-feldspar and apatite. Cordierite is present in migmatites but not in two-mica granites. This is reflected in the chemical composition since two-mica granites show a different REE pattern, higher K and P content and Rb/Sr ratio; (4) the isotopic signature of two-mica granites, migmatites and SGC metasediments shows a genetic link between them.

Like leucosomes and leucogranites, two-mica granites and diatexites also show replacement of plagioclase by K-feldspar. There are two types of k-feldspar crystals: one type is magmatic (euhedral to subhedral) and the other is anhedral always replacing plagioclase. Besides, Na + Ca and K content are uncorrelated. This is due to the different anatectic processes that originate these last lithologies: they incorporate all the components resulting from anatectic reactions plus restites, while leucogranites resulted from melt segregations and the restitic portion is subordinate. Also the diatexite and two-mica granite resulted from higher melting rate and formed in deeper levels.

It seems that multiple fluid pulses affected the MMC in subsolidus conditions: a first pulse with boron-bearing fluids and a second pulse containing silica-bearing aqueous-fluids. The occurrence of leucogranites and two-mica granites showing localized replacement of biotite by tourmaline, late tourmaline in the metasediments and the occurrence of pegmatite veins with abundant tourmaline suggest that late boron-rich fluids affected the MMC and surrounding metasedimentary sequence.

The entrainment of later silicate aqueous fluids is inferred from: (1) the muscovitization of tourmaline, biotite and plagioclase all over the MMC; (2) presence of quartz-veins cutting all the lithologies; (3) large quartz-crystals bands in some calc-silicate rocks that include all the previous rock-forming minerals; (4) retrograde alteration of staurolite, andalusite and biotite in the metasedimentary sequence.

Conclusion

The lithological, petrographic and geochemical aspects suggest the following anatexis/crystallization events:

(i) From a protolith consisting of SGC metasediments a first fluid-present melting mainly of

plagioclase and quartz produced some leucosomes and mostly leucogranites. These melts were formed under tectonic stress which led to their rapid migration and subsequent crystallization in dilatant sites. After the water available has been consumed fluid-absent breakdown of biotite reactions produced peritectic cordierite and leucosomes composed of plagioclase + quartz with minor amounts of K-feldspar. These processes occurred at relatively shallow levels at P<4 kPa;

(ii) At deeper levels (still below 4 kbar) and slightly high temperature, melt rate was greater and produced diatexites that intruded metatexites;

(iii) Above 4 kbar large amounts of melt were produced. The resultant melts are less dense than the host rocks, which promotes its ascent and emplacement at shallow levels, generating two-mica granites that incorporate migmatite xenoliths and form intrusive dikes.

At subsolidus conditions, the MMC was affected by boron-rich fluids that promoted the development of tourmaline in some leucogranites and two-mica granites and the installation of aplite-pegmatite veins that cut all the other lithologies and have isotopic signature quite different from them. The last silica-rich aqueous fluid pulse, probably in the continuity of the previous one, promoted the muscovitization of tourmaline, biotite, andalusite and staurolite in migmatites and surrounding metasediments.

It is suggested that the migmatization probably started after the compressional and crustal thickening stage of Variscan Orogeny and was continuously active during the following stage of deformation and D_3 transcurrent shearing since the main migmatite foliation is concordant with the main foliation in metasedimentary sequence (S_1) and the D_3 stress and structures conditioned the segregation, migration and emplacement of melts. The several pulses of different fluids that affected the MMC probably are related to the crystallization of syn and late-D_3 granites.

ACKNOWLEDGMENTS

This work was developed in the scope of the Centro de Geologia (University of Porto) activities with financial support of EU funds (FEDER – "Operacional Potencial Humano" Program) and Portuguese funds from FCT – "Fundação para a Ciência e Tecnologia" (research fellowship n° SFRH / BD / 65509 / 2009 and PETROCHRON - PTDC/CTE-GIX/112561/2009). We are grateful to Carlos Villaseca and Beatriz Valle Aguado whose comments greatly helped to improve the manuscript.

References

Ábalos, B.; Carreras, J.; Druguet, E.; Escuder Viruete, J.; Gómez Pugnaire, M.T.; Lorenzo Álvarez, S.; Quesada, C.; Rodríguez Fernández, L.R. & Gil Ibarguchi, J.I. (2002). Variscan and pre-Variscan tectonics. In: The Geology of Spain. (Gibbons, W. & Moreno, M.T., eds.), Geological Society, London, 155–183.

Areias M.; Ribeiro, M. A. & Dória, A. (2012). Metasomatized calc-silicate resisters in migmatites (Variscan Orogen, NW Portugal). First European Mineralogical Conference, Frankfurt, Germany, September, 2012, EMC2012-561.

Azevedo, M.R. & Valle Aguado, B. (2013). Origem e instalação de granitóides variscos na Zona Centro-Ibérica. In: Geologia de Portugal, Volume I- Geologia Pré-mesozóica de Portugal (Dias, R.; Araújo, A.; Terrinha, P. & Kullberg, J.C., eds.), Escolar Editora, Lisboa, 377–401.

Barbero, L. & Villaseca, C. (1995). Geochemical and isotopic disequilibrium in crustal melting: An insight from anatectic granitoides from Toledo, Spain. Journal of Geophysical Research: Solid Earth, 100: 15,745–15,765. http://dx.doi.org/10.1029/95JB00036.

Bea, F. (1996). Residence of REE, Y, Th and U in granites and crustal protoliths: Implications for the chemistry of crustal melts. Journal of Petrology, 37: 521–552. http://dx.doi.org/10.1093/petrology/37.3.521.

Bea, F. & Montero, P. (1999). Behavior of accessory phases and redistribution of Zr, REE, Y, Th, and U during metamorphism and partial melting of metapelites in the lower crust: An example from the Kinzigite Formation of Ivrea-Verbano, NW Italy. Geochimica et Cosmochimica Acta, 63: 1133–1153. http://dx.doi.org/10.1016/S0016-7037(98)00292-0.

Bea, F.; Montero, P. & Zinger, T. (2003). The Nature, Origin and Thermal Influence of the Granite Source Layer of Central Iberian Zone. Journal of Geology, 111: 579–595. http://dx.doi.org/10.1086/376767.

Beetsma, J.J. (1995). The late Proterozoic/Paleozoic and Hercynian crustal evolution of the Iberian Massif, N Portugal. PhD thesis, Vrije University, Netherlands, 223 pp.

Boynton, W.V. (1984). Geochemistry of rare earth elements: meteorite studies. In: Rare earth element geochemistry (Henderson, P., ed.), Elsevier, Netherlands, 63–114. http://dx.doi.org/10.1016/B978-0-444-42148-7.50008-3.

Brown, M. (2008). Granites, migmatites and residual granulites: relationships and processes. In: Working with migmatites (Sawyer, E. W., ed.). Mineralogical Association of Canada, Quebec, 97–114.

Brown, M. (2013). Granite: From genesis to emplacement. Geological Society of America Bulletin, 125 (7–8): 1079–1113. http://dx.doi.org/10.1130/B30877.1.

Capdevila, R.; Corretgé, L. & Floor, P., (1973). Les granitoides varisques de la Meseta Ibérique. Bulletin de la Société Géologique de France, 15: 209–228.

Casquet, C.; Fuster, J.M.; González-Casado, J.M.; Peinado, M. & Villaseca, C. (1988). Extensional tectonics and granite emplacement in the Spanish Central System – A discussion. In: Fifth EGT Workshop: The Iberian Peninsula (Banda, E. & MendesVictor, L.A., eds.), European Science Foundation, Estoril, 65–75.

Catalán, J.M.; Pascual, J.; Montes, A.; Fernández, R.; Barreiro, J.; Silva, I.; Clavijo, E.; Ayarza, P. & Alcock, J. (2014). The late Variscan HT/LP metamorphic event in NW and Central Iberia: relationships to crustal thickening, extension, orocline development and crustal evolution. In: The Variscan Orogeny: Extent, Timescale and the Formation of the European Crust (Schulmann, K., Catalán, J.R.M., Lardeaux, J.M., Janousek, V. & Oggiano, G., eds), Geological Society, London, Special Publications, 405: 225–247. http://dx.doi.org/10.1144/SP405.1.

Conrad, W.K.; Nicholls, I.A. & Wall, V.J. (1988). Water saturated and undersaturated melting at 10 kbar: evidence for the origin of silicic magmas in the Taupo volcanic zone, New Zealand, and other occurences. Journal of Petrology, 29: 765–803. http://dx.doi.org/10.1093/petrology/29.4.765.

Díez Balda, M.A.; Catalán, J.R.M. & Ayarza Arribas, P., 1995. Syn-collisional extensional collapse parallel to the orogenic trend in a domain of steep tectonics: the Salamanca Detachment Zone (Central Iberian Zone, Spain). Journal of Structural Geology, 17: 163–182. http://dx.doi.org/10.1016/0191-8141(94)E0042-W.

El Bouseily, A.M. & El Sokkary, A.A. (1975). The relation between Rb, Ba and Sr in granitic rocks. Chemical Geology, 16 (3): 207–219. http://dx.doi.org/10.1016/0009-2541(75)90029-7.

Escuder Viruete, J.; Arenas, R. & Catalán, J.R.M. (1994). Tectonothermal evolution associated with Variscan crustal extension in the Tormes Gneiss Dome (NW Salamanca, Iberian Massif, Spain). Tectonophysics, 238: 117–138. http://dx.doi.org/10.1016/0040-1951(94)90052-3.

Ferreira, N.; Iglésias, M.; Noronha, F.; Pereira, E.; Ribeiro, A. & Ribeiro, M.L. (1987). Granitoides da Zona Centro Ibérica e seu enquadramento geodinâmico. In: Geología de los Granitoides y Rocas Asociadas del Macizo Hespérico (Bea, F.; Carnicero, J.; Lopez Plaza, M. & Rodrigues Alonso, M., Eds.), Editorial Rueda, Madrid, 37–51.

García-Casco, A.; Torres-Roldan, R.L.; Millan, G.; Monie, P. & Haissen, F. (2001). High-grade metamorphism and hydrous melting of metapelites in the Pinos terrane (W Cuba): evidence for crustal thickening and extension in the northern Carribean collisional belt. Journal of Metamorphic Geology, 19: 699–715. http://dx.doi.org/10.1046/j.0263-4929.2001.00343.x.

García-Moreno, O.; Corretgé, L.G. & Castro A. (2007). Processes of assimilation in the genesis of cordierite leucomonzogranites from the Iberian Massif: a short review. The Canadian Mineralogist, 45: 71–85. http://dx.doi.org/10.2113/gscanmin.45.1.71.

Harris, N.B.W. & Inger, S. (1992). Trace element modelling of pelite derived granites. Contributions to Mineralogy and Petrology, 110: 46–56. http://dx.doi.org/10.1007/BF00310881.

Jung, S. (2005). Isotopic equilibrium/disequilibrium in granites, metasedimentary rocks and migmatites (Damara orogen, Namibia) - A consequence of polymetamorphism and melting. Lithos, 84: 168–184. http://dx.doi.org/10.1016/j.lithos.2005.03.013.

Martínez, F.J.; Reche, J. & Arboleya, M.L. (2001). P-T modelling of the andalusite-kyanite-andalusite sequence and related assemblages in high-Al graphitic pelites. Prograde and retrograde paths in a late kyanite belt in the Variscan Iberia. Journal of Metamorphic Geology, 19: 661–677. http://dx.doi.org/10.1046/j.0263-4929.2001.00335.x.

Martins, H.C.B.; Sant'Ovaia, H.; Abreu, J.; Oliveira, M., & Noronha, F. (2011). Emplacement of the Lavadores granite (NW Portugal). U/Pb and AMS results. Comptes Rendus Geoscience, 343(6): 387–396. http://dx.doi.org/10.1016/j.crte.2011.05.002.

McLennan, S. M. (1989). Rare earth elements in sedimentary rocks: influence of provenance and sedimentary processes. Reviews in Mineralogy, 21: 169–200.

Milord, I.; Sawyer, E.W. & Brown, M. (2001). Formation of diatexite migmatite and granite magma during anatexis of semipelitic metasedimentary rocks: An example from St. Malo, France. Journal of Petrology, 42: 487–505. http://dx.doi.org/10.1093/petrology/42.3.487.

Noronha, F.; Cathelineau, M.; Boiron, M.C.; Banks, D.A.; Dória, A.; Ribeiro, M.A.; Nogueira, P. & Guedes, A. (2000). A three stage fluid flow model for Variscan gold metallogenesis in northern Portugal. Journal of Geochemical Exploration, 71 (2): 209–224. http://dx.doi.org/10.1016/S0375-6742(00)00153-9.

Noronha, F.; Ramos, J.M.F.; Rebelo, J.A.; Ribeiro, A. & Ribeiro, M.L. (1979). Essai de correlation des phases de deformation hercynienne dans le Nord-Ouest Péninsulaire. Boletim da Sociedade Geológica de Portugal, 21(2/3): 227–237.

Noronha, F.; Ribeiro, M.A.; Almeida, A.; Dória, A.; Guedes, A.; Lima, A.; Martins, H.C.; Sant'Óvaia, H.; Nogueira, P.; Martins, T.; Ramos, R.; Vieira, R. (2013). Jazigos Filonianos Hidrotermais e Aplito-pegmatíticos Espacialmente Associados a Granitos (Norte de Portugal). In: Geologia de Portugal, Volume

I - Geologia Pré-mesozóica de Portugal (Dias, R.; Araújo, A.; Terrinha, P. & Kullberg, J.C., Eds.), Escolar Editora, Lisboa: 403–438.

Patiño Douce, A.E., & Harris, N. (1998). Experimental constraints on Himalayan anatexis: Journal of Petrology, 39: 689–710. http://dx.doi.org/10.1093/petroj/39.4.689.

Pereira, E.; Ribeiro A.; Carvalho, G.; Noronha F.; Ferreira N. & Monteiro J. H. (1992). Notícia Explicativa da Carta Geológica de Portugal na escala de 1:200 000. Serviços Geológicos de Portugal, 83 pp.

Pereira, M.D. & Bea, F. (1994). Cordierite-producing reactions in the Peña Negra Complex, Avila batholith, Central Spain: The key role of cordierite in low-pressure anatexis. The Canadian Mineralogist, 32: 763–780.

Pereira, M.F.; Linnemann U.; Hofmann M.; Chichorro M.; Solá A.R.; Medina J. & Silva, J.B. (2012). The provenance of Late Ediacaran and Early Ordovician siliciclastic rocks in the Southwest Central Iberian Zone: Constraints from detrital zircon data on northern Gondwana margin evolution during the late Neoproterozoic. Precambrian Research, 195: 166–189. http://dx.doi.org/10.1016/j.precamres.2011.10.019.

Ribeiro, A.; Munhá, J.; Dias, R.; Mateus, A.; Pereira, E.; Ribeiro, L.; Fonseca, P.; Araújo, A.; Oliveira, T.; Romão, J.; Chaminé, H.; Coke, C. & Pedro, J. (2007). Geodynamic evolution of SW Europe Variscides. Tectonics, 26: TC6009. http://dx.doi.org/10.1029/2006TC002058.

Ribeiro, M.A.; Dória, A. & Sant'Ovaia, H. (2008). Relações entre deformação, magmatismo e metamorfismo na região oriental do maciço do Porto. In: Resumos alargados. 8ª Conferencia Anual do Grupo de Geologia Estrutural e Tectónica. Sociedade Geológica de Portugal, 39–43.

Romão, J.; Metodiev, R. & Ribeiro, A. (2013). Evolução Geodinâmica dos sectores meridionais da Zona Centro-Ibérica. In: Geologia de Portugal, Volume I - Geologia Pré-mesozóica de Portugal (Dias, R.; Araújo, A.; Terrinha, P. & Kullberg, J.C., Eds.), Escolar Editora, Lisboa: 205–257.

Sousa, M. (1984). Considerações sobre a estratigrafia do Complexo Xisto-Grauváquico (CXG) e a sua relação com o Paleozóico Inferior. Cuadernos de Geología Ibérica, 9: 9–36.

Teixeira C. & Medeiros A.C. (1965). Notícia explicativa da Carta Geológica à escala 1/50.000, Folha 9A-Póvoa de Varzim, Serviços Geológicos de Portugal.

Teixeira R.J.S., (2008). Mineralogia, petrologia e geoquímica dos granitos e seus encraves da região de Carrazeda de Ansiães. Tese Universidade de Trás-os-Montes e Alto Douro-Vila Real. 430 pp.

Teixeira, R.; Neiva, A.; Gomes, M.E.; Corfu, F.; Cuesta, A. & Croudace, I.W. (2012). The role of fractional crystallization in the genesis of early syn-D3, tin-mineralized Variscan two-mica granites from the Carrazeda de Ansiães area, northern Portugal. Lithos, 153: 177–191. http://dx.doi.org/10.1016/j.lithos.2012.04.024.

Ugidos, J.M.; Sánchez-Santos, J.M.; Barba, P. & Valladares, M.I. (2010). Upper Neoproterozoic series in the Central Iberian, Cantabrian and West Asturian Leonese Zones (Spain): Geochemical data and statistical results as evidence for a shared homogenized source area. Precambrian Research, 178: 51–58. http://dx.doi.org/10.1016/j.precamres.2010.01.009.

Ugidos, J.M.; Valladares, M.I.; Barba, P. & Ellam, R.M. (2003). The Upper Neoproterozoic-Lower Cambrian of the Central Iberian Zone, Spain: chemical and isotopic (Sm-Nd) evidence that the sedimentary succession records an inverted stratigraphy of its source. Geochimica and Cosmochimica Acta, 67 (14): 2615–2629. http://dx.doi.org/10.1016/S0016-7037(03)00027-9.

Valladares, M.I.; Barba, P.; Ugidos, J.M.; Colmenero, J.R. & Armenteros, I. (2000). Upper Neoproterozoic-Lower Cambrian sedimentary successions in the Central Iberian Zone (Spain): sequence stratigraphy petrology and chemostratigraphy. Implications for other European zones. International Journal of Earth Sciences, 89: 2–20. http://dx.doi.org/10.1007/s005310050314.

Valle Aguado, B.; Azevedo, M.R.; Santos, J.F. & Nolan, J. (2010). O Complexo Migmatítico de Mundão (Viseu, norte de Portugal). e-Terra, 16: 9.

Valle Aguado, B.; Azevedo, M.R.; Schaltegger, U.; Catalán, J.R.M. & Nolan, J. (2005). U-Pb zircon and monazite geochronology of Variscan magmatism related to syn-convergence extension in Central Northern Portugal. Lithos, 82: 169–184. http://dx.doi.org/10.1016/j.lithos.2004.12.012.

Watson, E.B. (1996). Dissolution, growth and survival of zircons during crustal fusion: Kinetic principles, geological models and implications for isotopic inheritance. Transactions of the Royal Society of Edinburgh: Earth Sciences, 87: 43–56. http://dx.doi.org/10.1017/S0263593300006465.

Watt, G.R.; Burns, I.M. & Graham, G.A. (1996). Chemical characteristics of migmatites: Accessory phase distribution and evidence for fast melt segregation rates. Contributions to Mineralogy and Petrology, 125: 100–111. http://dx.doi.org/10.1007/s004100050209.

White, R.W. (2008). Insights into Crustal Melting and the Formation of Migmatites Gained from the Petrological Modeling of Migmatites. In: Working with migmatites (Sawyer, E. W., ed.). Mineralogical Association of Canada, Quebec, 77–96.

Zeng, L.; Asimow, P.D. & Saleeby, J.B. (2005a). Coupling of anatectic reactions and dissolution of accessory phases and the Sr and Nd isotope systematics of anatectic melts from a metasedimentary source.

Geochimica et Cosmochimica Acta, 69: 3671–3682. http://dx.doi.org/10.1016/j.gca.2005.02.035.

Zeng, L.; Saleeby, J.B. & Ducea, M. (2005b). Geochemical characteristics of crustal anatexis during the formation of migmatite at the Southern Sierra Nevada, California. Contributions to Mineralogy and Petrology, 150: 386–402. http://dx.doi.org/10.1007/s00410-005-0010-2.

Zhao, J.X.; McCulloch, M.T. & Bennett, V.C. (1992). Sm/Nd and U/Pb zircon isotopic constraints on the provenance of sediments from the Amadeus Basin, central Australia: Evidence for REE fractionation. Geochimica and Cosmochimica Acta, 56: 921–940. http://dx.doi.org/10.1016/0016-7037(92)90037-J.